Journal of Nuclear Engineering

MDPI

Article

Processing and properties of sintered W/steel-composites for the first wall of future fusion reactor

Vishnu Ganesh [1,*], Daniel Dorow-Gerspach [1], Martin Bram [1,2], Jan Willem Coenen [1], Marius Wirtz [1], Gerald Pintsuk [1], Werner Theisen [2] and Christian Linsmeier [1]

[1] Forschungszentrum Jülich GmbH, Institut für Energie- und Klimaforschung, 52425 Jülich Germany
[2] Institut für Werkstoffe, Lehrstuhl Werkstofftechnik, Ruhr-Universität Bochum, 44801 Bochum, Germany
* Correspondence: v.ganesh@fz-juelich.de

Abstract: Functionally graded tungsten/steel-composites may be used as an interlayer to join tungsten (W) and steel for the first wall of future fusion reactor to reduce the thermally induced stresses arising from the different coefficient of thermal expansion (CTE) of W and steel. W/steel-composites, with three W contents: 25, 50 and 75 vol% W, will serve as individual sublayers of this functionally graded material and gradually change the CTE from W to steel. Therefore, the present work exploits an emerging sintering technique, field assisted sintering technology, to produce these composites. The work presents, at first, the results of a process parameters optimization study to manufacture composites with lowest porosity and lowest amount of intermetallic compounds. The optimized composites 25, 50 and 75 vol% W achieved a relative density of 99 %, 99 % and 96 % respectively; measured via Archimedes' principle. Then, a high temperature mechanical test reveals that these composites are ductile above 300 °C. Lastly, the measured CTE, specific heat capacity and thermal conductivity were consistent with the theoretically expected values.

Keywords: W/steel-composites; FAST/SPS; First wall; Thermal analysis; Mechanical analysis

1. Introduction

The joining of tungsten (W) and steel for the first wall of a future fusion reactor is challenging due to the mismatch in their coefficient of thermal expansion (CTE), which generates thermal stress peaks at their interface. A promising solution would be to introduce a functionally graded material (FGM), made of W/steel-composites with varying volume concentration of W, as an interlayer to gradually change the CTE [1–3]. According to numerical calculations, a FGM consisting of three sublayers (25, 50, 75 vol% W) is a sensible compromise with regard to the manufacturing effort and stress reduction [1]. A potential route to manufacture these composites is via field assisted sintering technology/spark plasma sintering (FAST/SPS). FAST/SPS is an advanced powder metallurgy process that utilizes resistance heating and mechanical pressure to consolidate metallic or ceramic powders in a shorter time as compared to conventional powder metallurgy process [4–6]. Thus, in this work, W/steel-composites with three different volume concentrations of W (25, 50 and 75 vol%) were manufactured. The aim of this work was to produce and characterize dense composites with lowest amount of detrimental brittle intermetallic compounds (IMC). Therefore, firstly, the influence of sintering parameters, consolidate's thickness and particle size fraction (PSF) of the starting powders were investigated. Secondly, optimized parameters were found out and optimized composites were manufactured. Finally, mechanical and thermophysical analysis on these optimized composites were performed considering its application as a FGM interlayer.

2. Materials and Methods

2.1. Powder preparation

Citation: To be added by editorial staff during production.

Academic Editor: Firstname Lastname

Received: date
Accepted: date
Published: date

Spherical W and steel powders were used as the starting material. Two batches of W powders were purchased: one from China Tungsten Online (Xiamen) Manu. & Sales Corp, China and the other from Tekna Advanced Materials, Canada. The PSF of the powders were +10/-30 μm and +30/-60 μm respectively. The D_{50} were ~17 μm and ~50 μm respectively. Similarly, two batches of steel powders were purchased from Nanoval GmbH & Co. KG, Germany. The first batch had PSF of +10/-20 μm and D_{50} of 13 μm, the second batch had PSF of +3/-13 μm and D_{50} of 7 μm. The elemental composition of the steel powders was similar to that of a reduced activation martensitic/ferritic steel (Eurofer 97) [7–9]. The powder handling was done in an inert atmosphere glove box to prevent the oxidation of powders. The mixing of the powders was done as follows: the respective powders of desired PSF were weighed accordingly and filled in a plastic container, which was then sealed (inside the glove box) to maintain an inert atmosphere. Then, this container was removed out of the glove box and mounted in a tumble mixer and mixed for 72 hours to obtain homogenously mixed powders. Scanning electron microscopy (SEM) images of some of the mixed powders are given in supplementary information A.

2.2. Sintering methodology

The Sintering was performed using a lab scale FAST/SPS equipment (HP D-5 from FCT Systeme GmbH) using graphite tools (die and punches). The diameter of the die and punches was 20 mm. The tools were fabricated from an isostatically pressed graphite material (ISOSTATIC 2334 from MERSEN, France) of compressive strength 230 MPa. The geometry of the punch was optimized to withstand a pressure of 125 MPa.

The mixed powder was filled in this die and then pre-pressed to 125 MPa pressure. The powder and the die were separated by a 0.025 mm thick molybdenum foilto reduce the diffusion of carbon from the graphite tools to the composite material [10]. The sintering was performed under medium vacuum (~ 0.1 mbar). The pulse ON/OFF times of the pulsed DC current for the FAST/SPS cycle were 25 ms/5 ms respectively. The temperature was monitored and controlled using a vertical pyrometer pointed at the bottom of bore in the punch. The heating rate was 100 K/min. The temperature was kept constant after reaching the desired sintering temperature for the desired amount of time (sintering time). At the end of the sintering time, the current was switched off enabling the sample to cool down rapidly.

Three compositions were sintered starting from 25 vol% W, as represented in **Table 1**. For simplicity, 25 vol% W, 50 vol% W and 75 vol% W are labelled as 25W, 50W and 75W respectively. Sintering parameters (PSF, temperature, time and pressure) were optimized to achieve high densification. Moreover, the 25W was sintered for different consolidate's thicknesses in order to study its effect. The cross-section of the sintered composite was investigated by SEM images; the residual porosity and IMC were determined by image analysis. SEM micrographs were taken at different magnifications to include meso- and micro-scaled features; its mean value represents here the amount of porosity/IMC and its standard deviation represents an error band.

Table 1. PSF of the W and steel powders for different compositions.

Composition	Nomenclature	PSF of W	PSF of steel
25W	$25W_{10\text{-}30}+75S_{10\text{-}20}$	+10/-30 μm	+10/-20 μm
50W	$50W_{10\text{-}30}+50S_{10\text{-}20}$	+10/-30 μm	+10/-20 μm
	$50W_{10\text{-}30}+50S_{3\text{-}13}$	+10/-30 μm	+3/-13 μm
75W	$75W_{30\text{-}60}+25S_{10\text{-}20}$	+30/-60 μm	+10/-20 μm

2.3. Characterization of composites

After the optimization of sintering parameters, composites with these optimized parameters were freshly sintered and then these composites were further characterized. For the characterizations, specimens were cut using wire electric discharge machining.

2.3.1. Mechanical characterization

4-point bending tests were performed on specimens of size 12 mm x 1 mm x 1 mm at 20 °C, 100 °C, 300 °C and 550 °C (under vacuum). The flexural stress (σ_f) and strain (ε_f) were calculated based on ASTM D7265/D7264M [11]. For correct interpretation of the results, it must be noted that the formula used for stress and strain calculation is only valid in the elastic regime. Furthermore, there is no standard for performing bending tests on such small specimens, so these stress-strain curves must be read with care.

2.3.2. Thermophysical characterization

The density and the relative density of the composites was measured using Archimedes' principle with the help of Ethanol fluid. The thermophysical characterizations were done by performing the following tests as described in **Table 2**: dilatometer, dynamic differential scanning calorimetry (DSC), and laser flash analysis (LFA). These tests were performed to determine the following respective quantities: CTE, specific heat capacity (c_p) and thermal conductivity (λ). All the tests were performed under Ar atmosphere.

Table 2. Overview of thermophysical tests and testing conditions.

Test	**Equipment**	**Specimen** ***(mm)***	**Temperature** ***(°C)***
Dilatometer	LV75 from LINSEIS	4 x 2 x 15	20 to 1000
DSC	DSC 404 F3 from NETZSCH	Ø 5 x 1.5	20 to 1000
LFA	LFA427 from NETZSCH	10 x 10 x 1.5	20, 200, 400, 600, 800, 1000

The measured quantities were compared to their theoretical expected values. The theoretical expected secant CTE (α_{comp}) and specific heat capacity ($c_{p,comp}$) for different volume concentration of W (V_W) were calculated according to **Eq. 1** and **Eq. 2** respectively [1–3,12]. α_W and $\alpha_{Eurofer97}$ are the secant CTEs, ρ_W and $\rho_{Eurofer97}$ are the densities, $c_{p,W}$ and $c_{p,Eurofer97}$ are the specific heat capacities of pure W and Eurofer 97 steel, respectively [13–15].

$$\alpha_{comp}(V_W, T) = V_W \alpha_W(T) + (1 - V_W)\alpha_{Eurofer97}(T) \quad (1)$$

$$c_{p,comp}(V_W, T) = \frac{c_{p,W}(T)\rho_W V_W + c_{p,Eurofer97}(T)\rho_{Eurofer97}(1 - V_W)}{\rho_W V_W + \rho_{Eurofer97}(1 - V_W)} \quad (2)$$

Unlike CTE and c_p, there is no specific relation to predict the theoretical thermal conductivity of such composites as it depends predominantly on the spatial microstructural arrangement of W and steel constituents. Therefore, simple upper ($\lambda_{upper-bound,comp}$) and lower bound ($\lambda_{lower-bound,comp}$) models were suggested here to compare the measured values (see **Eq. 3** and **Eq. 4)** [1,16]. Here, λ_W and $\lambda_{Eurofer97}$ represent the thermal conductivity of pure W and Eurofer 97 steel, respectively [13,14].

$$\lambda_{upper-bound,comp}(V_W, T) = V_W \lambda_W(T) + (1 - V_W)\lambda_{Eurofer97}(T) \quad (3)$$

$$\lambda_{lower-bound,comp}(V_W, T) = \left(\frac{1 - V_W}{\lambda_{Eurofer97}(T)} + \frac{V_W}{\lambda_W(T)}\right)^{-1} \quad (4)$$

3. Results and discussion

3.1. Optimizing the sintering parameters for 25W

Figure 1 (a) indicates the porosities of the 25W composites sintered at three sintering temperatures for a sintering time of 5 min and at a pressure of 50 MPa. The thicknesses of the sintered composites were also varied to 0.75 mm, 2 mm and 3 mm. The increase in temperature results in the decrease of residual porosity. For the composite sintered at 900 °C, the majority of pores were present inside the steel matrix and with the increase of sintering temperature these pores close down. The residual porosity for composite sintered at 1100 °C reduced to less than 1 %, but resulted in high amount of IMC (~ 6 %). These IMCs were not only present at the W-steel interfaces but also in regions close to W particles, mostly along the grain boundaries of the steel matrix. For thinner composites (2 mm and 0.75 mm), the increase in temperature from 1000 °C to 1100 °C played no significant effect on the residual porosity. For a sintering temperature of 1000 °C, the reduction in consolidate's thickness from 3 mm to 2 mm clearly reduced the residual porosity to less than 1 %. It is also worth mentioning that, in these composites some occasional occurrence of bigger pores (~ 3 to 4 μm) were also found inside the steel matrix even though the overall residual porosity was less than 1 %. This reduction in porosity with the reduction in consolidate's thickness is due to wall friction effect which reduces the active powder compaction pressure for thicker consolidate.

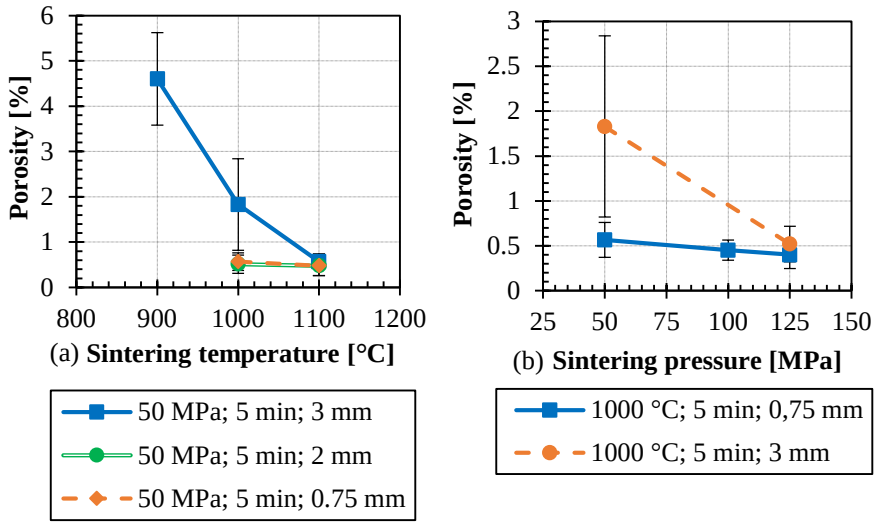

Figure 1. Residual porosity of sintered 25W composites: (a) Effect of sintering temperature and consolidate's thickness; (b) Effect of sintering pressure and consolidate's thickness.

Furthermore, in order to understand the effect of sintering pressure, the sintering was also performed at higher pressure (125 MPa) as shown in **Figure 1** (b). For thicker consolidate (3 mm), the pressure significantly improves the consolidation by suppressing the wall friction effect. Based on these results, the optimum sintering parameter for 25W composite was found to be 1000 °C, 125 MPa, and 5 min and the cross-section of an optimized sintered 25W composite is shown in **Figure 2.** Additional SEM micrographs are provided in supplementary information B.

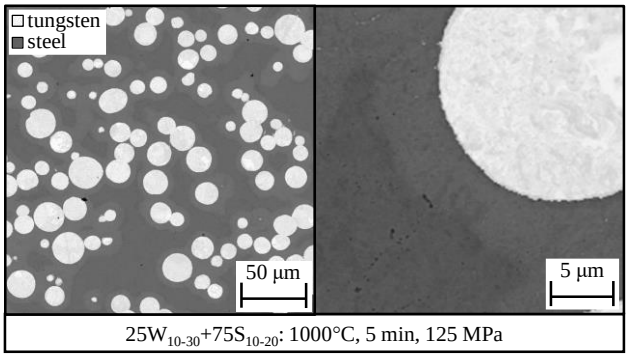

Figure 2. Cross sectional SEM micrograph of 25W composite sintered with optimized parameter.

3.2. Optimizing the sintering parameter for 50W

At first, the composition $50W_{10\text{-}30}+50S_{10\text{-}20}$ was sintered at temperatures between 900°C and 1100°C at 50 MPa for time of 5 min. Also, based on the results of 25W composites only two consolidate's thicknesses were considered (3 mm and 0.75 mm). Here as well the increase in the sintering temperature resulted in better densification as seen in **Figure 3** (a). But the porosity for the 3 mm thick composite sintered at 1000 °C was still high (7 %). Increasing the temperature to 1100 °C reduced the porosity but resulted in higher amount of IMC (~ 14.87 %). For the sintering temperature of 1000 °C, even the decrease of the composite's thickness from 3 mm to 0.75 mm did not improve the residual porosity. This implied that increasing the pressure would not lead to any sort of improvement.

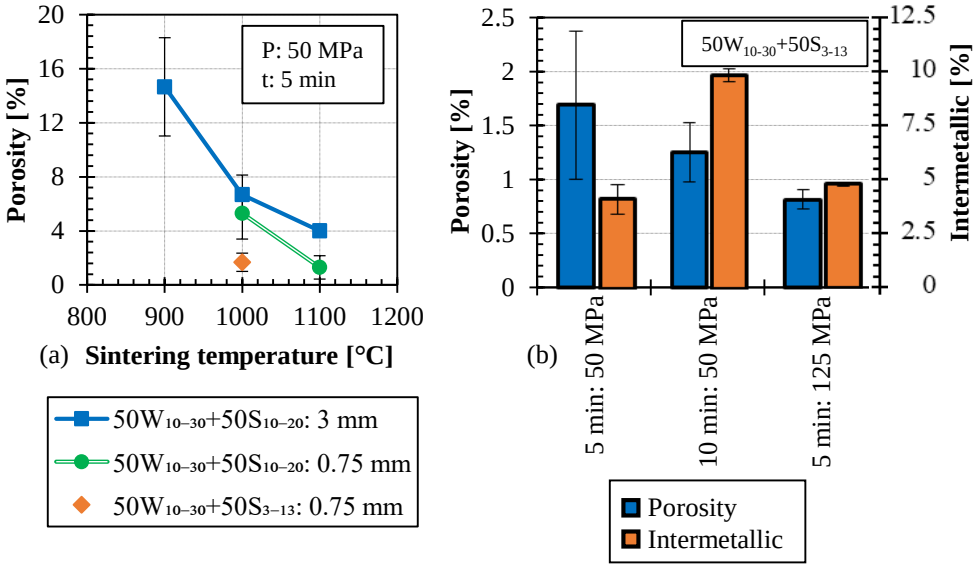

Figure 3. Residual porosity of sintered 50W composites; (a) Effect of sintering temperature and consolidate's thickness as well as the effect of 50W composition ($50W_{10\text{-}30}+50S_{10\text{-}20}$ and $50W_{10\text{-}30}+50S_{3\text{-}13}$): (b) Effect of sintering time and pressure for the 50W composition ($50W_{10\text{-}30}+50S_{3\text{-}13}$).

In order to keep the sintering temperature limited to 1000 °C (same as that of the optimized parameter for 25W), another composition with finer steel powder, $50W_{10\text{-}30}+50S_{3\text{-}13}$, was investigated. In this case, a residual porosity of 1.6 % was already achieved at 1000 °C, 5 min, 50 MPa for a sample thickness of 0.75 mm as seen in Figure 3 (a). Doubling the sintering time to 10 min led to a minor reduction of porosity, but the amount of IMC increased from 4.12 % to 9.86 % as seen in **Figure 3** (b). When the pressure was increased to 125 MPa, the residual porosity reduced to less than 1 % while the amount of IMC remained almost the same. Therefore, the optimized parameters for

sintering the 50W composite were found to be 1000 °C; 125 MPa; 5 min and using the $50W_{10\text{-}30}+50S_{3\text{-}13}$ composition and the corresponding optimized composite is shown in **Figure 4**. Additional SEM micrographs are provided in supplementary information B.

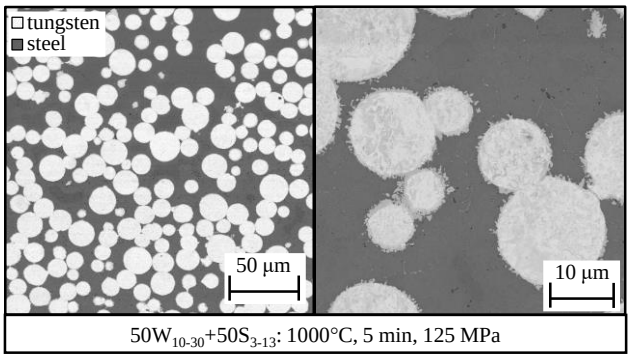

Figure 4. Cross sectional SEM micrograph of 50W composite sintered with optimized parameter.

3.3. Optimizing the sintering for 75W

The 75W composition contains 75 vol% W and this makes the sintering process challenging because of two reasons: Firstly, the presence of higher amount of W particles mean that the composite would contain more W-W contact points and generally the metallurgical bonding of W-W particles is difficult. Secondly, usually a higher sintering temperature in the range of 1800 °C to 2000 °C is required to sinter pure W using FAST/SPS process [17]. However, at such a high temperature the steel would melt and lower temperature would result in higher number of unbonded W-W particles. Previous studies on the sintering of W/steel-composite via a similar electric field assisted sintering process revealed that for higher volume concentration of W, the sintered composites contain higher amount of unbonded W-W particles. Hence, considering all these challenges a coarser W powder of size +30/-60 µm instead of +10/-30 µm was used to reduce the amount of W-W particle contacts.

Thus, the resulting composition $75W_{30\text{-}60}+25S_{10\text{-}20}$ was sintered at various sintering temperature between 1000 °C and 1400 °C for a sintering time of 5 min. As seen in **Figure 5**, as the sintering temperature increases the porosity decreases but at the same time the amount of IMC also increases. It is not trivial to determine the optimized sintering parameters for 75W composite; Firstly, at lower sintering temperature the porosity is higher, but at higher sintering temperature the amount of IMC is higher. Secondly, the sintering parameters for the 75W composite should be the same as for 25W and 50W in order to produce the whole FGM in one step. Therefore, the optimized parameter set for 75W was also considered to be 1000 °C, 5 min at 125 MPa and the microstructure of the corresponding composite is shown in **Figure 6**. The left-hand side SEM micrograph shows that the composite is dense enough but, in some regions (as seen in the right-hand side SEM), the composite has higher porosity. Also, some of the W-W particles do not form any metallurgical bonding as represented by the red mark. Nevertheless, this composite will serve as the topmost 75W sublayer of the FGM. Additional SEM micrographs are provided in supplementary information C.

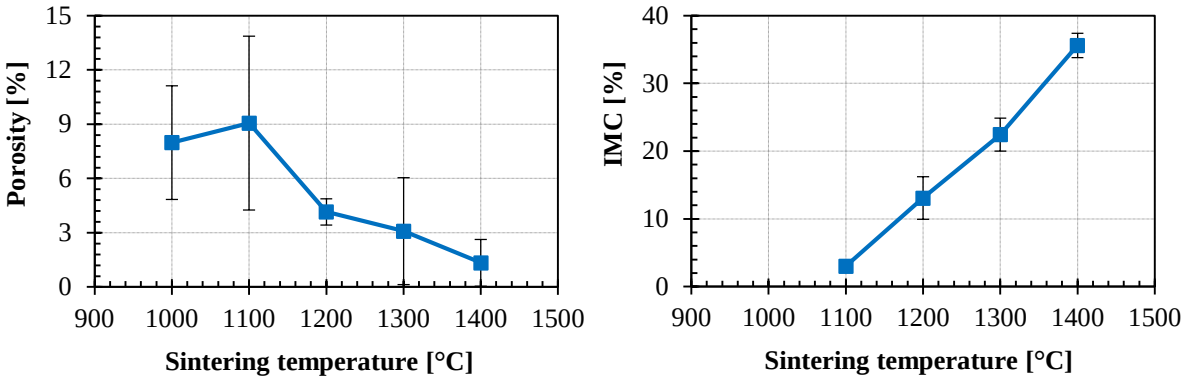

Figure 5. Porosities and IMC of 75W composites sintered at different temperatures.

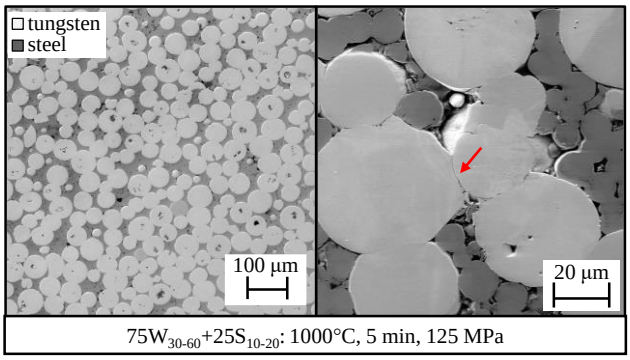

Figure 6. Cross sectional SEM micrograph of 75W composite sintered with optimized parameter.

3.4. Properties of the composites

3.4.1. Comprehensive microstructural analysis

The conventional mechanical grinding and polishing process for the metallographic investigation doesn't reveal intricate details, therefore in order to get a perfectly polished surface focused ion beam cuts were made. The corresponding SEM micrographs (**Figure 7)** showing individual phases along with their elemental composition, determined by energy-dispersive X-ray spectroscopy (EDX), as listen in **Table 3**. Following inferences were made based on this analysis:

- Firstly, in all composites W-steel interface forms a thin (~ 100 nm) compound of composition $Fe_xW_yCr_z$ as confirmed by the EDX analysis (EDX-5). The values of EDX-5 should be read with care since the thickness of this compound is lower than the excitation area of EDX.
- Secondly, nano-scale voids are present inside the steel matrix.
- Thirdly, in 25W composite (Figure 7 (a)) the steel matrix close to W particle formed a ferritic (α) phase. This phase was formed because of the diffusion of W from the W-particle to the steel matrix. This resulted in around 8.9 wt% W inside this region as listed by EDX-3 in Table 3. As W is a ferrite stabilizer this region does not form martensitic during cool down but becomes ferritic. In the case of 50W composite (Figure 7 (b)), most of the steel phase became ferritic because of this interdiffusion of W (EDX-4). In the case of 75W composite as well (Figure 7 (c)), most of the steel matrix was found to be ferritic.
- Fourthly, in 25W composite the steel matrix further away from the W particle retains its original chemical composition as listed by EDX-2. This elemental composition is same to that of Eurofer 97 steel, which is a martensitic steel [8]. The SEM micrograph is this region clearly shows a martensitic phase structure. This was further confirmed by the cooling rate during the sintering process; the cooling rate between

1000 °C and 400 °C was found to be 210 K/min which is significantly higher than the critical cooling rate (~5 K/min) to accomplish martensitic transformation [8,18].

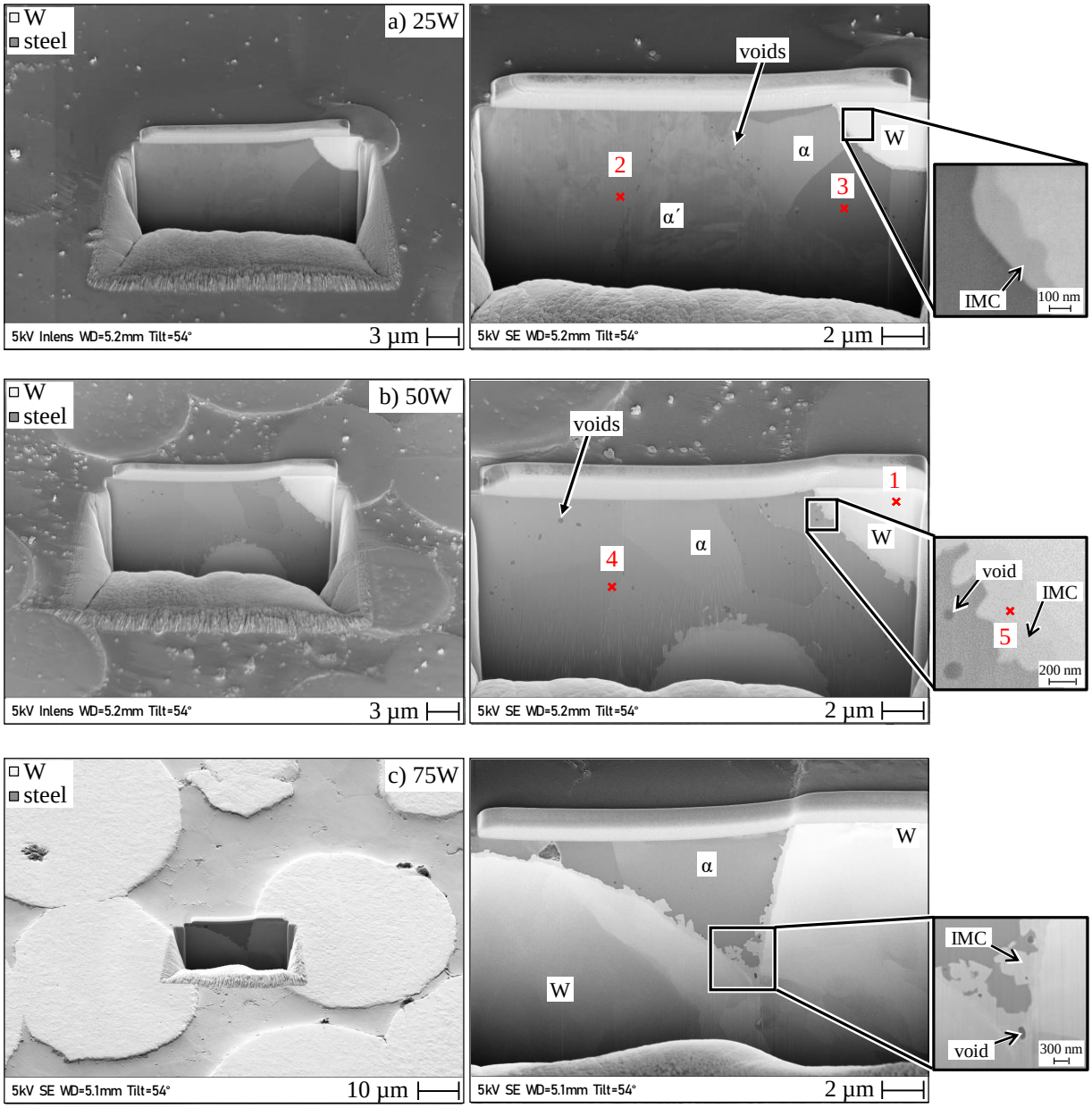

Figure 7. Comprehensive SEM micrographs showing individual phases: (a) 25W; (b) 50W; (c) 75W.

Table 3. EDX spectrum analysis at different locations marked in Figure 7.

EDX spectrum *(wt%)*	Fe	Cr	W	V	Mn	Ta
EDX-1	0.5	-	99.5	-	-	-
EDX-2	88.8	8.9	1.6	0.3	0.3	0.1
EDX-3	82.8	8.3	8.3	0.2	0.4	-
EDX-4	82.3	7.9	9.4	0.2	0.2	-
EDX-5	31.9	4.3	63.6	0.1	0.1	-

Note: It should be noted that EDX analysis was not performed on the FIB-cuts itself, but they were done on regions away from the FIB-cuts. The marks in Figure 7 are intended to clarify the phases on which the measurements were made. Also, carbon is selected as a deconvolution element.

3.4.2. Mechanical properties

The flexural stress-strain curves of composites are shown in Figure 8. The 25W specimens tested at 300 °C and 550 °C did not fracture but the test had to be stopped at around 8 % flexural strain since this was the upper limit of the testing setup. The 50W and 75W composites were less ductile, however above 300 °C the 50W and 75W showed appropriate ductility and failed at around 3 % and 1 % flexural strain respectively. Above 550 °C, both 50W and 75W showed excellent ductility and failed at around 4 % flexural strain. Moreover, the maximum flexural strength of 50W and 75W is significantly lower than that of 25W. The strength of 75W was slightly higher than that of 50W but still comparatively less than that of 25W. This is because of the weak bonding between W particles. This implies that increasing the amount of W-W bonds in the W-steel composites is detrimental for the mechanical properties resulting in early failure.

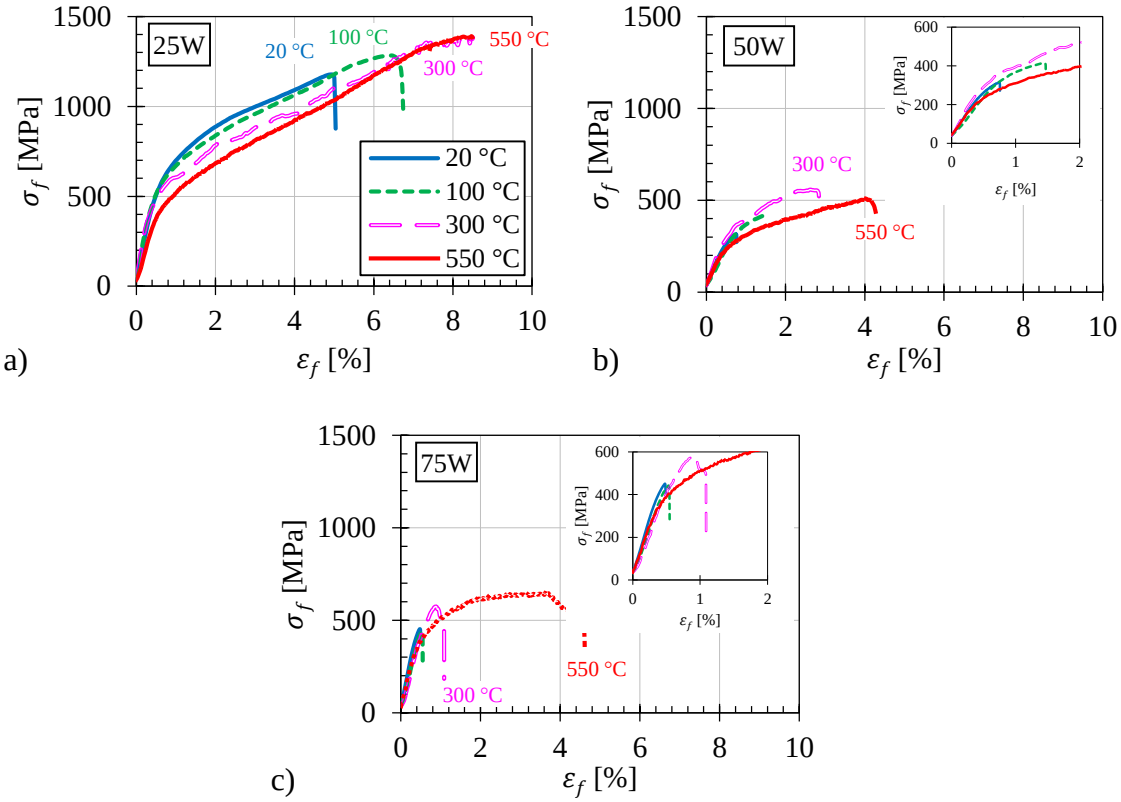

Figure 8. Flexural stress vs strain curves for: (a) 25W; (b) 50W; (c) 75W composite.

3.4.3. Thermophysical properties

The density measured by Archimedes' principle is shown in **Figure 9**. The relative density of the composites shows that the composites are dense including the 75W as it has a relative density of 96 %. The measured (mea.) secant CTE and specific heat capacity of the composites show a good agreement with the theoretical (th.) values as shown in **Figure 10**. The CTE of the composites gradually change from 25W to 75W and the values are within that of pure W and pure Eurofer 97 steel. The c_p curve shows a clear curie transition peak at around 750 °C for all composites. Additionally, the intensity of the peak matches with the amount of steel present in the specimen.

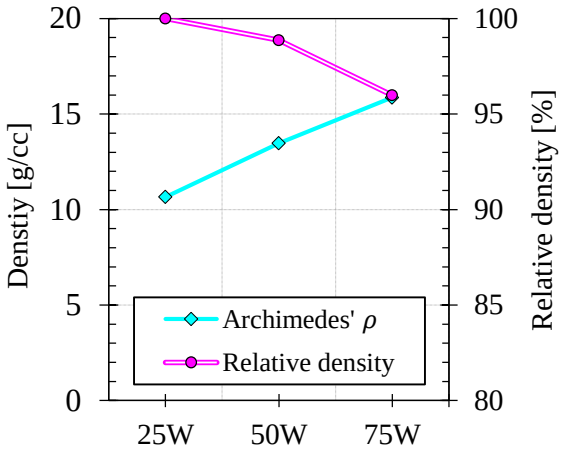

Figure 9. Archimedes' density and their corresponding relative density.

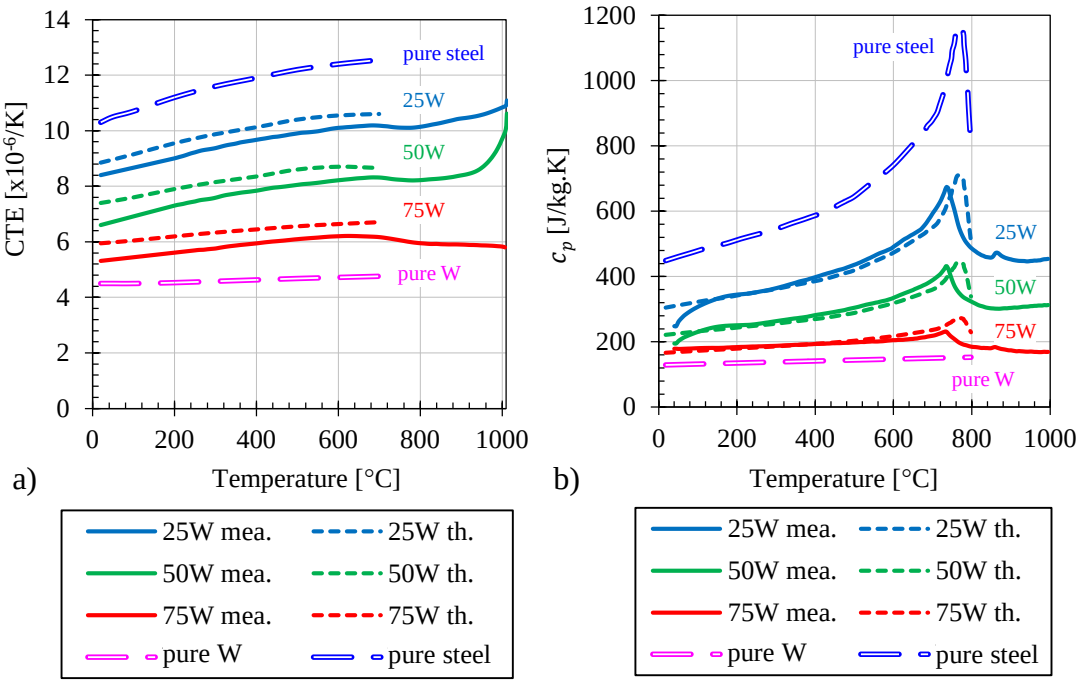

Figure 10. (a) Secant CTE; (b) Specific heat capacity of the composites in comparison to their theoretical values. In addition, values of pure W and pure Eurofer 97 steel [13–15].

The measured thermal conductivities of the composites are more inclined towards the theoretical lower bound values or even below as shown in **Figure 11**. For the 25W and 50W composites, despite having a relative density of 99 % the thermal conductivities follow a lower bound value. This is because of the spatial arrangement of the W particles; the W particles are mostly surrounded by the steel matrix which is analogues to a metal matrix composite with W particles being embedded inside the steel matrix. This implies that the heat must follow steel and W successively (one after the other) and the formula which predicts the lower bound values are suitable for composites in which the heat follows the constituents successively. Therefore, for 25W and 50W composites the lower bound model is more suitable. In the case of 75W, the temperature dependency of the thermal conductivity follows the theoretical upper bound model i.e. is dominated by the W contribution. However, the absolute values are much lower than the predicted ones. This implies a large thermal resistance within the material due to the weak or even non-existing bonding between W particles.

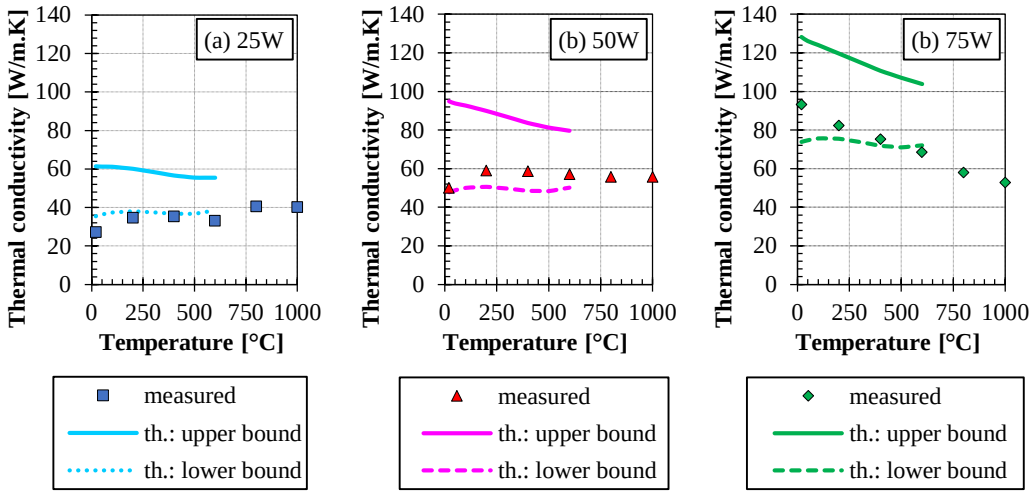

Figure 11. Measured and theoretically expected lower and upper bound values: (a) 25W; (b) 50W; and (c) 75W composite.

4. Conclusions

In the present work, FAST/SPS technique was used to manufacture W-steel composites with three W concentrations: 25, 50 and 75 vol% W (25W, 50W and 75W). These composites will be used as a stress relieving functionally graded (FGM) interlayer for W-steel joining. Optimum sintering parameters have been found in this comprehensive study to be 1000 °C 125 MPa, and 5 min. The optimized 25W and 50W composites were successfully manufactured with less than 1 % porosity. Using the same parameters also for 75W resulted in a relative density of 96 %. The optimized composites also contained low amount of brittle intermetallic compounds. Microstructural analysis of composites revealed the presence of martensite and ferrite phases in the steel matrix. The thermophysical properties of the composites agree very well with theoretical values calculated on the basis of simple rules of mixtures. The CTE of the composites gradually varies according to the volume concentration of W, which means that these composites are suitable to be used as sublayers of the FGM. The thermal conductivities of the composites agreed well with the expected theoretical lower bound values and were higher than that of pure Eurofer 97 steel. However, despite the high relative density of the 50W and 75W composite, their flexural mechanical properties were worse than that of 25W composite. Nevertheless, all composites still showed a reasonable ductility above 300 °C; it must be pointed out that the temperature of the coolant in the first wall will be about 300 °C and this means the lowest temperature such composites would undergo during operation is 300 °C. This further implies that such composites would withstand the thermal stresses occurring during the thermal cycling in a future fusion reactor. As an intermediate step, a complete graded FGM was also sintered by placing the 25W, 50W and 75W premixed powders on top of each other and sintering at the optimized sintering parameter. A cross-sectional overview is provided in the supplementary information C. Furthermore, the gained knowledge and properties of the composites would help to understand the potential application of such FGM interlayer and would help the future work to assess the possibility to join W and steel using this FGM.

Supplementary Materials: The following supporting information can be downloaded at: www.mdpi.com/xxx/s1, Figure S1: title; Table S1: title; Video S1: title.

Author Contributions: "Conceptualization, V.G. and D.D.; methodology, V.G. and D.D.; investigation, V.G.; resources, M.B.; writing—original draft preparation, V.G.; writing—review and editing, V.G., D.D. and M.B.; supervision, D.D., W.T.; project administration, C.L.; funding acquisition, J.W., M.W. and G.P."

Acknowledgments: This work has been carried out within the framework of the EUROfusion Consortium, funded by the European Union via the Euratom Research and Training Programme (Grant Agreement No 101052200 –EUROfusion). Views and opinions expressed are however those of the author(s) only and do not necessarily reflect those of the European Union or the European Commission. Neither the European Union nor the European Commission can be held responsible for them. The authors would like to thank the following people for their assistance: Ms. Beatrix Göths for FIB-cuts, Mr. Rudi Caspers for specimen cutting, Mr. Philipp Lied and Mr. Siegfried Baumgärtner for bending test.

Conflicts of Interest: "The authors declare no conflict of interest". "The funders had no role in the design of the study; in the collection, analyses, or interpretation of data; in the writing of the manuscript; or in the decision to publish the results".

References

1. Heuer, S.; Weber, T.; Pintsuk, G.; Coenen, J.W.; Matejicek, J.; Linsmeier, C. Aiming at understanding thermo-mechanical loads in the first wall of DEMO: Stress-strain evolution in a Eurofer-tungsten test component featuring a functionally graded interlayer. *Fusion Eng. Des.* **2018**, *135*, 141–153, doi:10.1016/j.fusengdes.2018.07.011.
2. Weber, T.; Aktaa, J. Numerical assessment of functionally graded tungsten/steel joints for divertor applications. *Fusion Eng. Des.* **2011**, *86*, 220–226, doi:10.1016/j.fusengdes.2010.12.084.
3. Qu, D.; Basuki, W.W.; Aktaa, J. Numerical assessment of functionally graded tungsten/EUROFER coating system for first wall applications. *Fusion Eng. Des.* **2015**, *98-99*, 1389–1393, doi:10.1016/j.fusengdes.2015.06.120.
4. Guillon, O.; Gonzalez-Julian, J.; Dargatz, B.; Kessel, T.; Schierning, G.; Räthel, J.; Herrmann, M. Field-Assisted Sintering Technology/Spark Plasma Sintering: mechanisms, materials, and technology developments. *Adv. Eng. Mater.* **2014**, *16*, 830–849, doi:10.1002/adem.201300409.
5. Mamedov, V. Spark plasma sintering as advanced PM sintering method. *Powder Metall.* **2002**, *45*, 322–328, doi:10.1179/003258902225007041.
6. Orru, R.; Licheri, R.; Locci, A.M.; Cincotti, A.; Cao, G. Consolidation/synthesis of materials by electric current activated/assisted sintering. *Mater. Sci. Eng. R Rep.* **2009**, *63*, 127–287, doi:10.1016/j.mser.2008.09.003.
7. van der Schaaf, B.; Tavassoli, F.; Fazio, C.; Rigal, E.; Diegele, E.; Lindau, R.; Le Marois, G. The development of EUROFER reduced activation steel. *Fusion Eng. Des.* **2003**, *69*, 197–203, doi:10.1016/S0920-3796(03)00337-5.
8. Rieth, M.; Schirra, M.; Falkenstein, A.; Graf, P.; Heger, S.; Kempe, H.; Lindau, R.; Zimmermann, H. *EUROFER 97*: *Tensile, charpy, creep and structural tests*. Wissenschaftliche Berichte, FZKA-6911, Karlsruhe, 2003 (accessed on 18 February 2021).
9. Tanigawa, H.; Shiba, K.; Möslang, A.; Stoller, R.E.; Lindau, R.; Sokolov, M.A.; Odette, G.R.; Kurtz, R.J.; Jitsukawa, S. Status and key issues of reduced activation ferritic/martensitic steels as the structural material for a DEMO blanket. *J. Nucl. Mater.* **2011**, *417*, 9–15, doi:10.1016/j.jnucmat.2011.05.023.
10. Kwak, N.; Min, G.; Oh, Y.; Suh, D.-W.; Kim, H.C.; Kang, S.; Han, H.N. Tantalum and molybdenum barriers to prevent carbon diffusion in spark plasma sintered tungsten. *Scr. Mater.* **2021**, *196*, 113759, doi:10.1016/j.scriptamat.2021.113759.
11. ASTM Standard D30; D30 Committee. *Standard test method for flexural properties of polymer matrix composite materials // Test Method for Flexural Properties of Polymer Matrix Composite Materials*: *Designation: D7264/D7264M-07;* ASTM International: West Conshohocken, PA.
12. Heuer, S.; Coenen, J.W.; Pintsuk, G.; Matejicek, J.; Vilemova, M.; Linsmeier, C. Overview of challenges and developments in joining tungsten and steel for future fusion reactors. *Physica Scripta* **2020**, *T171*, 14028, doi:10.1088/1402-4896/ab47a4.
13. ITER. *Materials Properties Hanbook (MPH)*: *ITER Doc. G74 MA 16 04-05-07 R0.1.*, 2017.
14. EUROfusion. *DEMO Material Property Handbook (MPH)*: *EUROFER 97*.
15. Tavassoli, A.A.F.; Alamo, A.; Bedel, L.; Forest, L.; Gentzbittel, J.M.; Rensman, J.W.; Diegele, E.; Lindau, R.; Schirra, M.; Schmitt, R.; et al. Materials design data for reduced activation martensitic steel type EUROFER. *J. Nucl. Mater.* **2004**, *329-333*, 257–262, doi:10.1016/j.jnucmat.2004.04.020.
16. Heuer, S. Charakterisierung gradierter Eisen/Wolfram-Schichten für die erste Wand von Fusionsreaktoren. PhD dissertation; Ruhr-Universität Bochum, Bochum, Germany, 2017.
17. Matejicek, J.; Veverka, J.; Yin, C.; Vilemova, M.; Terentyev, D.; Wirtz, M.; Gago, M.; Dubinko, A.; Hadraba, H. Spark plasma sintered tungsten – mechanical properties, irradiation effects and thermal shock performance. *J. Nucl. Mater.* **2020**, *542*, 152518, doi:10.1016/j.jnucmat.2020.152518.
18. Lindau, R.; Schirra, M. First results on the characterisation of the reduced-activation-ferritic-martensitic steel EUROFER. *Fusion Eng. Des.* **2001**, *58-59*, 781–785, doi:10.1016/S0920-3796(01)00562-2.